Bipolar resistive switching in an amorphous zinc tin oxide memristive device

Jaana S. Rajachidambaram
School of Chemical, Biological and Environmental Engineering, Oregon State University, Corvallis, Oregon 97331

Santosh Murali and John F. Conley, Jr.
School of Electrical Engineering and Computer Science, Oregon State University, Corvallis, Oregon 97331

Stephen L. Golledge
Center for Advanced Materials Characterization in Oregon, University of Oregon, Eugene, Oregon 97403

Gregory S. Herman[a)]
School of Chemical, Biological and Environmental Engineering, Oregon State University, Corvallis, Oregon 97331

(Received 9 August 2012; accepted 24 October 2012; published 27 November 2012)

The integration of amorphous zinc tin oxide (ZTO) into crossbar memristor device structures has been investigated where asymmetric devices were fabricated with Al (top) and Pt (bottom) electrodes. The authors found that these devices had reproducible bipolar resistive switching with high switching ratios $>10^4$ and long retention times of $>10^4$ s. Electrical characterization of the devices suggests that both filamentary and interfacial mechanisms are important for device switching. The authors have used secondary ion mass spectrometry to characterize the devices and found that significant interfacial reactions occur at the Al/ZTO interface. © *2013 American Vacuum Society*. [http://dx.doi.org/10.1116/1.4767124]

I. INTRODUCTION

Advances in the development of transparent amorphous oxide semiconductors for thin film transistor (TFT) applications have made considerable progress since initial reports.[1–4] Benefits of these transparent amorphous oxide semiconductors include the ability to deposit them over large areas with uniform structural and electrical properties. Of increasing interest is the application of oxide materials for other devices including memristors and resistive random access memory (RRAM).[5,6] Recent results have demonstrated bipolar resistive switching for the transparent amorphous oxide semiconductor In-Ga-Zn-O (IGZO) in standard metal–insulator–metal (MIM) structures.[7–11] These results demonstrate the potential to integrate transparent amorphous oxide semiconductors for both TFT and memory, and may enable advanced system-on-panel display applications.

Although IGZO is the dominant transparent amorphous oxide semiconductor for TFT applications,[1] there is considerable interest in finding materials with similar performance, but without indium and gallium, which are increasingly expensive materials. Zn-Sn-O (ZTO) is a low-cost indium-free alternative transparent amorphous oxide semiconductor with excellent electrical properties for TFT applications.[3,12,13] Recently we have demonstrated bipolar resistive switching in solution-deposited ZTO memrsitors and found that the resistive switching was consistent with a combined filamentary/interfacial mechanism.[14] However, to better understand the switching mechanism for ZTO memristors we have fabricated devices using RF sputter-deposited ZTO in this study. RF sputter deposition allows excellent control over the electronic properties of ZTO films as we have recently demonstrated in a prior study for TFTs.[13] We have found that the bipolar resistive switching properties of the ZTO memristors were closely related to the electrical test conditions, and that an initial high current (>0.1 mA) forming step was not required to obtain reversible stable switching. The physical and electrical characterization of the ZTO materials and devices, along with the switching mechanisms will be discussed. Specifically, time-of-flight secondary ion mass spectrometer (ToF-SIMS) depth profiles indicate the presence of an interfacial AlO_x layer which appears to strongly influence the switching characteristics of the devices.

II. EXPERIMENT

Memristor crossbar devices were fabricated on thermally oxidized silicon substrates using standard MIM structures. All patterning was performed using photolithography and lift-off processes. The bottom 50 nm thick Pt electrode was deposited using an e-beam evaporator, where a 25 nm thick titanium adhesion layer was used at the Pt/SiO_2 interface. Just prior to ZTO deposition the substrates were rinsed with acetone, isopropyl alcohol, and deionized water, blow dried using nitrogen, and heated for 5 min at 100 °C on a hot plate to remove residual moisture from the surface. The 50 nm ZTO layer was deposited using RF magnetron sputter deposition. A 3-in. ZTO target with a $ZnO:SnO_2$ ratio of 2:1 (Zn_2SnO_4) was used. The ZTO films were deposited with 100 W power, a 20 SCCM flow rate with a 2:18 O_2:Ar ratio, and ~4 mTorr chamber pressure. No postdeposition annealing of the ZTO films was performed. The top ~200 nm thick Al electrode was deposited using a thermal evaporator. The crossbar structures had widths of 10, 20, 50, and 100 μm leading to crossbar cell areas of 100, 400, 2500, and

[a)]Author to whom correspondence should be addressed; electronic mail: greg.herman@oregonstate.edu

Downloaded 05 Mar 2013 to 128.193.162.72. Redistribution subject to AVS license or copyright; see http://avspublications.org/jvstb/about/rights_and_permissions

10 000 μm^2. The electrical switching characteristics were measured using a 4155 C Agilent semiconductor parameter analyzer and a probe station. All electrical measurements were performed at room temperature in the dark.

Sputter depth profiles were obtained with an ION-TOF IV ToF-SIMS using 1 keV Cs^+ ions for the sputter depth profile and 25 keV Bi^{3+} ions for analysis. For these studies, the positive secondary ions were analyzed. Spectroscopic ellipsometry was performed with a J. A. Woollam variable angle spectroscopic ellipsometer system with a rotating analyzer configuration to determine the ZTO optical properties and film thickness.

III. RESULTS AND DISCUSSION

Figure 1(a) shows the I-V characteristics of a typical Al/ZTO/Pt memristor showing bipolar resistive switching. For all measurements, the bottom electrode was grounded and the bias was applied to the top electrode. We have found that the devices were initially in the high resistance state (HRS) for the deposition conditions used in this study. When a negative voltage was applied to the top electrode, for a device in the HRS, there was a linear increase in current on a log-linear scale, as shown in the lower left side of the figure.

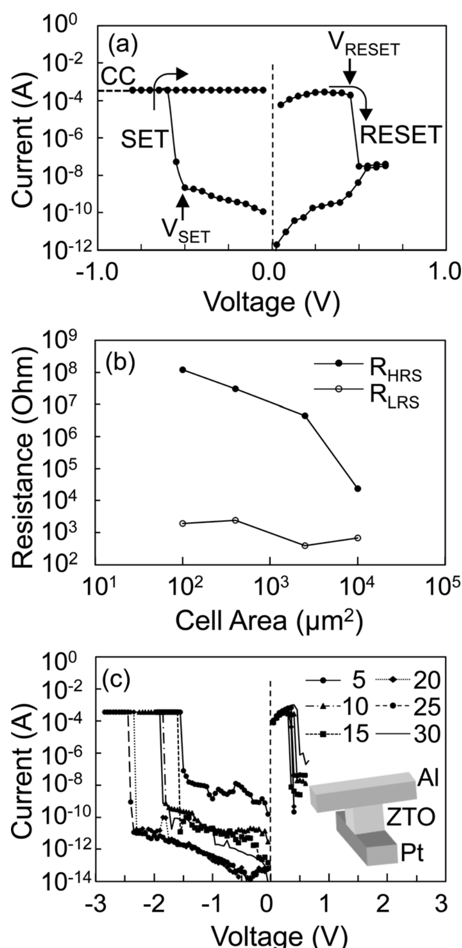

FIG. 1. (a) Typical bipolar resistive switching behavior for a ZTO memristor. (b) Dependence of R_{LRS} and R_{HRS} on cell area. (c) Bipolar resistive switching behavior for multiple cycles for a ZTO RRAM memristor; inset shows a schematic of the device stack.

At a certain voltage, there was a sharp increase in current as the device transitions from the HRS to the low resistance state (LRS). This is the SET process (device switched "on") and the voltage at which this transition takes place is defined as the SET voltage (V_{SET}). When a positive voltage was applied to the top electrode, for a device in the LRS, there was a transition back to the HRS, as shown in the upper right side of the figure. This transition is the RESET process (device switched "off"), and the voltage at which this transition takes place is defined as the RESET voltage (V_{RESET}). To avoid electrical breakdown of the devices, the compliance current (CC) was used during the SET process.[15,16] Previously, we found that a gradual forming process resulted in more uniform bipolar switching characteristics.[14] For the gradual forming process in the current study, the limiting CC was slowly increased in steps from 100 nA to 350 μA for a virgin device. This was continued until the devices transitioned from unipolar switching, which was initially observed for low CC, to bipolar switching.

Figure 1(b) shows the resistance change (R_{LRS} and R_{HRS}) with respect to the cell area. We found that R_{LRS} was nominally constant with increasing cell area while R_{HRS} decreased with increasing cell area. When R_{LRS} does not change with cell area, a dominate filament mechanism is invoked where conduction is dictated by locally confined filaments and not the area of the device.[7,17] When R_{HRS} does change with cell area bulk conduction, interfacial effects at the electrode–ZTO interface or noncontacting multifilament arrays are invoked where conduction is dictated by the area of the device.[15] Similar scaling behavior for R_{LRS} and R_{HRS} has been observed for other materials systems, including IGZO,[7] ZnO,[17] and MnO_2.[18] It should be noted that R_{HRS} for the three smallest devices has a slope of -1 with device area; however, the largest devices' R_{HRS} deviates from this expected relationship. The enhanced leakage for the largest devices may be related to extrinsic defects, and we did find a substantially lower yield for the largest devices. Figure 1(c) shows bipolar resistive switching for more than 30 cycles for a $20 \times 20\,\mu m^2$ Al/ZTO/Pt cross bar cell obtained after an initial gradual forming process and a CC of 350 μA. It can be seen that there was significant variation in V_{SET} while V_{RESET} stayed fairly constant. The values for mean of V_{SET} and V_{RESET} were determined to be -1.97 and 0.47 V with standard deviations of 0.57 and 0.34 V, respectively.

Figure 2(a) shows the change in R_{HRS} and R_{LRS} with respect to the number of switching cycles for the device characterized in Fig. 1(c). Despite the fluctuations of R_{HRS}, a resistance ratio (R_{HRS}/R_{LRS}) was $>10^4$ which is suitable for many memory applications.[6] To test the nonvolatility of the ZTO memristor, retention measurements were performed with a read voltage of 0.1 V for devices set in the HRS and LRS. Measurements were performed after various lengths of time to obtain the values for R_{HRS} and R_{LRS} as shown in Fig. 2(b). The values for R_{HRS}/R_{LRS} were $>10^4$ for longer than 10^4 s and did not show degradation during these measurements. This suggests that the ZTO memristor has excellent data retention, although longer tests should be performed on optimized devices to determine the data retention limit.

Downloaded 05 Mar 2013 to 128.193.162.72. Redistribution subject to AVS license or copyright; see http://avspublications.org/jvstb/about/rights_and_permissions

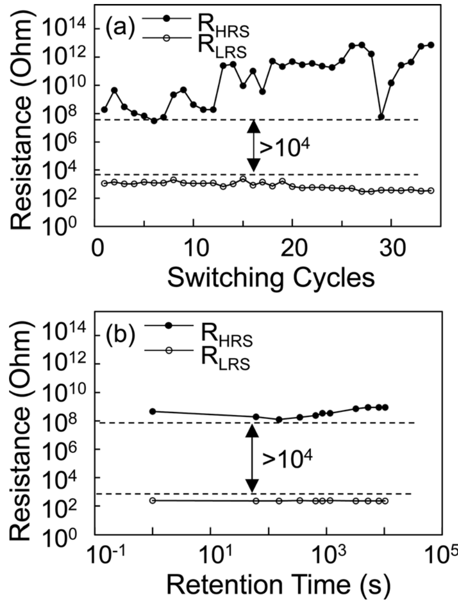

FIG. 2. (a) Dependence of R_{LRS} and R_{HRS} for 30 resistive switching cycles. (b) Retention characteristics of ZTO memristor taken with a read voltage of 0.1 V.

In order to better understand carrier transport in these devices, we have plotted log |I| vs log |V| for the LRS and HRS as shown in Fig. 3(a). At the low voltage region of both LRS ($V < V_{RESET}$) and HRS ($V > V_{SET}$), a linear increase with a slope of roughly 1 is observed suggesting Ohmic conduction. While for increasing negative biases, just below the V_{SET}, the HRS slope is found to increase substantially. To determine the current conduction mechanism in the high negative voltage region, we have considered both Schottky and Poole–Frenkel emission. Schottky emission (electron emission over a barrier) can be characterized by the following equation:[16]

$$\ln(I) \sim \left[\left(\frac{q^3}{\pi d \varepsilon_r \varepsilon_0}\right)^{\frac{1}{2}}\right] \frac{V^{\frac{1}{2}}}{2k_B T},$$

where q is electric charge, d is thickness of film, ε_r is dynamic dielectric constant, ε_0 is permittivity of free space, k_B is Boltzmann's constant, and T is the absolute temperature. By replotting the data as ln |I| vs $|V|^{1/2}$ in Fig. 3(b), the values for ε_r can be estimated by extracting from the slope of the graph. Likewise, Poole–Frenkel emission (electron conduction through traps) can be characterized by the following equation:[19]

$$\ln(I/V) \sim \left[\left(\frac{q^3}{\pi d \varepsilon_r \varepsilon_0}\right)^{\frac{1}{2}}\right] \frac{V^{\frac{1}{2}}}{k_B T}.$$

By replotting the data as ln |I/V| vs $|V|^{1/2}$ in Fig. 3(c), the values for ε_r can be estimated by extracting from the slope of the graph. To distinguish between Schottky and Poole–Frenkel emission for the devices, these extracted values of ε_r can be compared to the optical dielectric constant ($\varepsilon_{r,o}$) for ZTO. The value of $\varepsilon_{r,o}$ for ZTO was determined to be ~3.69 using the refractive index (n = 1.92) of the ZTO films obtained from ellipsometry and using the relation $n = \varepsilon_{r,o}^{1/2}$.[20,21]

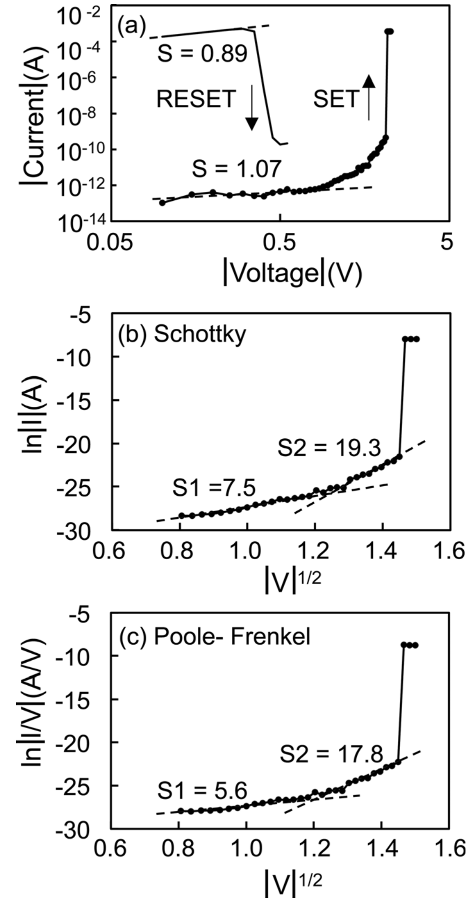

FIG. 3. (a) Plot of log |I| vs log |V| for the LRS and HRS of a typical device. The same data are plotted to evaluate Schottky and Poole–Frenkel emission in (b) and (c), respectively.

As shown in Figs. 3(b) and 3(c), the high voltage region of HRS ($V \leq V_{SET}$) has two linear regimes where there is a significant change in slope. The extracted values for ε_r were calculated using these two different slopes (S1 and S2) for both plots assuming either Schottky or Poole–Frenkel emission (see Table I). For Schottky emission, the extracted values for ε_r were significantly smaller than $\varepsilon_{r,o}$ for both S1 and S2 suggesting that Schottky emission can be eliminated as the conduction mechanism at these higher negative biases. For Poole–Frenkel emission, the extracted values for ε_r from region S1 gave a value fairly close to $\varepsilon_{r,o}$; however, the extracted value from region S2 was significantly lower than $\varepsilon_{r,o}$. This suggests that Poole–Frenkel emission is the dominant conduction mechanism in region S1; however, neither

TABLE I. Experimental values for optical dielectric constant (ε_r) for ZTO calculated using slopes (S1 and S2) of Schottky and Poole–Frenkel emission for high voltage regions ($V \leq V_{SET}$) of HRS. The optical dielectric constant $\varepsilon_{r,o}$ for ZTO was estimated to be ~3.69 from spectroscopic ellipsometry.

Region of analysis	ε_r Schottky	ε_r Poole–Frenkel
S1	0.78 ± 0.4	5.65 ± 2.5
S2	0.12 ± 0.1	0.55 ± 0.4

Downloaded 05 Mar 2013 to 128.193.162.72. Redistribution subject to AVS license or copyright; see http://avspublications.org/jvstb/about/rights_and_permissions

Schottky nor Poole–Frenkel emission adequately describes the data in region S2 (to be discussed in more detail below). In contrast, our prior ZTO memristor results had only a single slope in the high bias region, and also that Schottky emission was the dominant conduction mechanism.[14] These differences may be due to several factors including the initial electrical properties of the films (i.e., insulating for the sputter deposited and semiconducting for the solution deposited), or the difference in their relative thicknesses (i.e., 50 nm for sputter deposited and 6 nm for the solution deposited).

Figures 4(a) and 4(b) show ToF-SIMS depth profiles from ZTO memristors corresponding to a device that has been switched several cycles (now in HRS) and to a device that no longer switches (stuck in LRS), respectively. For these data, we have focused on the Al/ZTO interface since there were no major changes in the depth profile at the ZTO/Pt interface. For consistency, the relative intensities in the two figures have been normalized to the Al signal from the top metal electrode. In Fig. 4(a), we have identified an AlO_x interface layer (as indicated by the dashed box) for the device set in the HRS. This assignment is due to the increase of the oxygen signal prior to the increase in intensity of the zinc or tin signals from the ZTO film. The thickness of the AlOx layer was estimated to be ∼8–9 nm based on the sputter etch rates for the ToF-SIMS system. AlO_x interface layers were also observed in ToF-SIMS depth profiles for untested devices that were in the HRS. In Fig. 4(b), we did not observe a significant AlO_x interface layer (as indicated by the dashed box) for a device that failed by being stuck in the LRS. This assignment is due to the increase in the oxygen, zinc, and tin signals at the same point in the depth profile. These data indicate that significant interfacial reactions can occur between Al and ZTO, which can be expected based on the relative thermodynamic stabilities of the binary oxides that can form at this interface (e.g., Al_2O_3, ZnO, SnO_2, and SnO).[22] The formation of an insulating Al_2O_3 layer at the Al/ZTO interface likewise also forms a substoichiometric ZTO layer that will contain both oxygen vacancies and metal ion interstitials. Both of these defects in the ZTO film will result in a higher conductivity due to the higher carrier concentration than the stoichiometric ZTO. Recent studies have suggested that the interfacial reactions between reactive metal electrodes and the oxide switching material can strongly influence the I-V characteristics of the devices.[8,23–27]

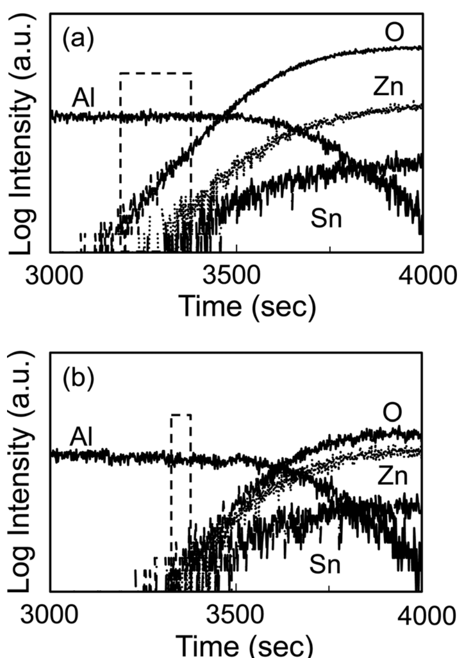

FIG. 4. ToF-SIMS depth profiles of two different devices. (a) Device in HRS and (b) device stuck in LRS.

In an earlier study, we have demonstrated that varying the partial pressure of oxygen during the deposition process can control the conductivity of as-deposited ZTO and that post-annealing the samples can significantly alter the chemistry at or near the surface.[13] X-ray photoelectron spectroscopy (XPS) results indicated that there is a significant amount of impurities at or near the surface of the films as judged by the carbon and oxygen core-level spectra. The O 1s and C 1s spectra for the unannealed ZTO samples (as used in this study) showed significantly higher levels of hydroxide, carbonate, and water than those annealed to 300 °C or higher.[13] Due to the deposition conditions used for this study, we expect that the films should initially be insulating since the addition of oxygen during ZTO sputter deposition process reduces the number of oxygen vacancies and metal interstitials in the ZTO films, resulting in a reduction of the carrier concentration. Furthermore, the hydroxide, carbonate, and water at the surface region of the ZTO films should readily react with the Al top metal electrode. ToF-SIMS indicates that an insulating AlO_x interface layer was formed by a reaction between Al and ZTO. This interfacial redox reaction results in the formation of both an insulating AlO_x region and a more conductive ZTO region as described above.

During the gradual forming process a negative voltage is applied to the Al top electrode, which may result in the drift of defect species in the AlO_x or ZTO films. Although this gradual forming process is at much lower currents than the electroforming process used for TiO_2 based devices,[28] the potential exists for Joule heating which may enhance diffusion and drift of these defect species. These defect species can include oxygen ions (negative charged) in the AlO_x layer, or oxygen vacancies (positive charged) in the ZTO layer, as has been reported for TiO_2 based memristors.[5] For TiO_2 based memristors, a significant change in the Al/TiO_2 interfacial layer thickness was observed using transmission electron microscopy whether a device was in the high (thickness ∼ 2.8 nm) or low (thickness ∼ 1.0 nm) resistive state.[29] The authors proposed that the uniform migration of oxygen ions into the TiO_2 films during the SET process reduces the thickness of the interfacial layer and results in the lower resistivity. It has been proposed by several groups that the redox based processes can lead to switching of memristive devices, where a negative voltage on a reactive electrode can lead to enhanced oxygen diffusion from the interfacial region leading to a reduction in the thickness of the interfacial oxide layer.[23,24,26] Although most studies focus on the drift of oxygen ions or vacancies, it is possible that metal cation species can drift under electric fields as has

Downloaded 05 Mar 2013 to 128.193.162.72. Redistribution subject to AVS license or copyright; see http://avspublications.org/jvstb/about/rights_and_permissions

been reported for IGZO TFTs.[30] The transport of oxygen ions, oxygen vacancies, or metal interstitials can change the relative conductivity of the interfacial region, but also an accumulation of these species can result in the formation of localized conductive filaments and the transition from the HRS to LRS during the SET process.[6,15,19] Alternatively, the devices can be returned to the HRS by application of a positive voltage at the Al electrode (RESET process). The switching to the HRS may be due to reduction/oxidation reactions that cause the dissolution of filaments in the Al/ZTO interface layer by the resulting drift of the defect species discussed above.

In general, our main failure mechanism was due to devices stuck in the LRS. This has also been observed for Ta_2O_5 devices as well,[31] where it is believed that the failure was related to extended stress in the base layer (medium resistivity TaO_{2-x} layer) or the interface of the metal-base or insulator-base layers as opposed to the switching layer (insulating Ta_2O_{5-x} layer). Our ToF-SIMS data for the device stuck in the LRS [Fig. 4(b)] indicate that there is an absence of an interfacial AlO_x layer, and also a relative change in the O, Zn, and Sn ion intensities compared to the device in the HRS [Fig. 4(a)]. It should be noted that these devices were located next to each other on the same die, and that these differences are not related to changes in the fabrication process. The absence of the interfacial AlO_x layer for the device stuck in the LRS suggests that either oxygen ions drift out of this layer, oxygen vacancies drift into this layer, or that metal interstitials drift into this layer. This process appears to be irreversible. In regards to the changes in the relative intensities of the ToF-SIMS depth profiles, it should be noted that SIMS ion yields are strongly influenced by relative atomic concentrations, sputter yield, ionization potential, and the chemical environment of the species.[32] Further studies on the role of metal contacts to the ZTO memristors need to be performed to better understand the switching mechanisms, as well as the relative ion yields in the ToF-SIMS data for ZTO devices. These results provide further evidence that an AlO_x interfacial layer contributes to the bipolar resistive switching observed for solution processed ZTO devices fabricated with the same structure.[14]

Finally, at high negative bias we believe that the increase in slope from region S1 to S2, as seen in Figs. 3(b) and 3(c), can be correlated to direct tunneling through this thin AlO_x layer. For applied negative voltages above -1.6 V, electrons in the Al electrode can tunnel directly through the thin AlO_x interfacial layer. It has been found that for electric fields between $\sim$1.5 and 6 MV/cm direct tunneling is the dominant mechanism electron conduction for thin Al_2O_3 films in MIM device structures.[33] This suggests that electron conduction in the high negative bias regime for the ZTO memristors, in this study, transition from Poole–Frenkel emission (region S1) to direct tunneling (region S2).

IV. CONCLUSIONS

In conclusion, memristors based on sputter-deposited ZTO have been investigated for nonvolatile memory applications. The as-deposited amorphous ZTO based RRAM devices had stable bipolar switching characteristics with a large R_{HRS}/R_{LRS} ratio $> 10^4$ and the HRS and LRS were found to be stable for retention times $>10^4$ s. The driving mechanism behind resistive switching was proposed to be due to combination of bulk effect (formation and dissolution of filamentary conduction paths) and an interface effect (redox reactions at the Al/ZTO interface). Based on ToF-SIMS data, we believe that the AlOx interfacial layer is critical for the observed bipolar resistive switching of the ZTO memristors, since devices that failed did not have this interfacial layer and were irreversibly stuck in the low resistive state.

ACKNOWLEDGMENTS

This research was performed, in part, using facilities at the Microproducts Breakthrough Institute and the Materials Synthesis and Characterization Facility at Oregon State University and the Center for Advanced Materials Characterization in Oregon at the University of Oregon. The project was funded by the Oregon Nanoscience and Microtechnologies Institute and the Office of Naval Research under Contract No. 200CAR262. Partial support for J.F.C. was also provided through the National Science Foundation through DMR-0805372. The authors thank K. Nishimura of Sharp Laboratories of America for assistance with device fabrication.

[1] T. Kamiya, K. Nomura, and H. Hosono, Sci. Technol. Adv. Mater. **11**, 044305 (2010).
[2] K. Nomura, H. Ohta, A. Takagi, T. Kamiya, M. Hirano, and H. Hosono, Nature **432**, 488 (2004).
[3] H. Q. Chiang, J. F. Wager, R. L. Hoffman, J. Jeong, and D. A. Keszler, Appl. Phys. Lett. **86**, 013503 (2005).
[4] N. L. Dehuff, E. S. Kettenring, D. Hong, H. Q. Chiang, J. F. Wager, R. L. Hoffman, C.-H. Park, and D. A. Keszler, J. Appl. Phys. **97**, 064505 (2005).
[5] D. B. Strukov, G. S. Snider, D. R. Stewart, and R. S. Williams, Nature **453**, 80 (2008).
[6] R. Waser, R. Dittmann, G. Staikov, and K. Szot, Adv. Mater. **21**, 2632 (2009).
[7] M.-C. Chen, T.-C. Chang, S.-Y. Huang, S.-C. Chen, C.-W. Hu, C.-T. Tsai, and S. M. Sze, Electrochem. Solid-State Lett. **13**, H191 (2010).
[8] M.-C. Chen, T.-C. Chang, C.-T. Tsai, S.-Y. Huang, S.-C. Chen, C.-W. Hu, S. M. Sze, and M.-J. Tsai, Appl. Phys. Lett. **96**, 262110 (2010).
[9] C. H. Kim, Y. H. Jang, H. J. Hwang, C. H. Song, Y. S. Yang, and J. H. Cho, Appl. Phys. Lett. **97**, 062109 (2010).
[10] M.-C. Chen *et al.*, Electrochem. Solid-State Lett. **14**, H475 (2011).
[11] Z. Q. Wang, H. Y. Xu, X. H. Li, X. T. Zhang, Y. X. Liu, and Y. C. Liu, IEEE Electron Device Lett. **32**, 10 (2011).
[12] W. B. Jackson, R. L. Hoffman, and G. S. Herman, Appl. Phys. Lett. **87**, 193503 (2005).
[13] J. S. Rajachidambaram, S. Sanghavi, P. Nachimuthu, V. Shutthanandan, T. Varga, B. Flynn, S. Thevuthasan, and G. S. Herman, J. Mater. Res. **27**, 2309 (2012).
[14] S. Murali, J. S. Rajachidambaram, S.-Y. Han, C.-H. Chang, G. S. Herman, and J. F. Conley, Jr., "Resistive switching in zinc-tin-oxide," Solid-State Electron. (2012).
[15] B. J. Choi *et al.*, J. Appl. Phys. **98**, 033715 (2005).
[16] X. Cao, X. M. Li, X. D. Gao, Y. W. Zhang, X. J. Liu, Q. Wang, and L. D. Chen, Appl. Phys. A **97**, 883 (2009).
[17] N. Xu, L. Liu, X. Sun, X. Liu, D. Han, Y. Wang, R. Han, J. Kang, and B. Yu, Appl. Phys. Lett. **92**, 232112 (2008).
[18] M. K. Yang, J.-W. Park, T. K. Ko, and J.-K. Lee, Appl. Phys. Lett. **95**, 042105 (2009).
[19] W. Y. Chang, Y. C. Lai, T. B. Wu, S. F. Wang, and F. Chen, Appl. Phys. Lett. **92**, 022110 (2008).
[20] X. Wu, P. Zhou, J. Li, L. Y. Chen, H. B. Lv, Y. Y. Lin, and T. A. Tang, Appl. Phys. Lett. **90**, 183507 (2007).

Downloaded 05 Mar 2013 to 128.193.162.72. Redistribution subject to AVS license or copyright; see http://avspublications.org/jvstb/about/rights_and_permissions

[21] D. S. Shang, L. D. Chen, Q. Wang, W. Q. Zhang, Z. H. Wu, and X. M. Li, Appl. Phys. Lett. **89**, 172102 (2006).
[22] C. T. Campbell, Surf. Sci. Rep. **27**, 1 (1997).
[23] Y. H. Do, J. S. Kwak, J. P. Hong, K. Jung, and H. Im, J. Appl. Phys. **104**, 114512 (2008).
[24] H. Y. Jeong, J. Y. Lee, S.-Y. Choi, and J. W. Kim, Appl. Phys. Lett. **95**, 162108 (2009).
[25] J. J. Yang, J. P. Strachan, F. Miao, M.-X. Zhang, M. D. Pickett, W. Yi, D. A. A. Ohlberg, G. Medeiros-Ribeiro, and R. S. Williams, Appl. Phys. A **102**, 785 (2011).
[26] C. Chen, F. Pan, Z. S. Wang, J. Yang, and F. Zeng, J. Appl. Phys. **111**, 01702 (2012).
[27] T. Bertaud *et al*., Thin Solid Films **520**, 4551 (2012).
[28] J. P. Strachan, D. B. Strukov, J. Borghetti, J. J. Yang, G. Medeiros-Ribeiro, and R. S. Williams, Nanotechnology **22**, 254015 (2011).
[29] H. Y. Jeong, J. Y. Lee, and S.-Y. Choi, Appl. Phys. Lett. **97**, 042109 (2010).
[30] J. Kang, K.-J. Moon, T. I. Lee, W. Lee, and J.-M. Myoung, Appl. Surf. Sci. **258**, 3509 (2012).
[31] M.-J. Lee *et al*., Nature Mater. **10**, 625 (2011).
[32] A. Benninghoven, F. G. Rüdenauer, and H. W. Werner, *Secondary Ion Mass Spectrometry: Basic Concepts, Instrumental Aspects, Applications, and Trends* (Wiley, New York, 1987).
[33] S. Meng, C. Basceri, B. W. Busch, G. Derderian, and G. Sandhu, Appl. Phys. Lett. **83**, 4429 (2003).

Downloaded 05 Mar 2013 to 128.193.162.72. Redistribution subject to AVS license or copyright; see http://avspublications.org/jvstb/about/rights_and_permissions